High-Performance Field-Effect Transistors Based on Polystyrene-*b*-Poly(3-hexylthiophene) Diblock Copolymers

Xiang Yu,[†] Kai Xiao,[‡,*] Jihua Chen,[‡] Nickolay V. Lavrik,[‡] Kunlun Hong,[‡,*] Bobby G. Sumpter,[‡] and David B. Geohegan[‡]

[†]Chemical Sciences Division,[‡]Center for Nanophase Materials Sciences, Oak Ridge National Laboratory, One Bethel Valley Road, Oak Ridge, Tennessee 37831, United States

ABSTRACT Polystyrene-*b*-poly(3-hexylthiophene) (PS-*b*-P3HT) block copolymers with fixed PS block length have been synthesized by combined atom transfer radical polymerization (ATRP) and Grignard metathesis (GRIM) polymerization. The self-assembled structures of these diblock copolymer thin films based on PS-*b*-P3HT have been studied by TEM, SAED, GIXD, AFM, and additionally by first principles modeling and simulation. These block copolymers undergo microphase separation and form nanostructured spheres, lamellae, nanofibers, or nanoribbons in the films dictated by the molecular weight of the P3HT block. Within the diblock copolymer thin film, PS blocks segregate to form amorphous domains, and the covalently bonded conjugated P3HT blocks exist as highly ordered crystalline domains through intermolecular packing with their alkyl side chains aligned normal to the substrate while the thiophene rings align parallel to the substrate through $\pi-\pi$ stacking. The conjugated PS-*b*-P3HT block copolymers exhibited significant improvements in organic field-effect transistor (OFET) performance and environmental stability as compared to P3HT homopolymers, with up to a factor of 2 increase in measured mobility (0.08 $cm^2/(V \cdot s)$) for the P4 (85 wt % P3HT). Overall, this work demonstrates that the high degree of molecular order induced by block copolymer phase separation can improve the transport properties and stability of conjugating polymers, which are critical for high-performance OFETs and other organic electronics.

KEYWORDS: self-assembly · conjugated diblock copolymer · organic field-effect transistors

To develop high-performance organic electronic devices, such as organic field-effect transistors (OFETs)[1−3] or organic photovoltaic devices (OPVs),[4] it is of crucial importance to control the nanostructures of semiconducting polymers.[5] Conjugated block copolymers are promising molecular architectures since they self-assemble into a variety of segregated nanoscale structures and can provide an opportunity to tailor the morphology of the active layer that enables charge carrier conduction within organic electronic devices.[6−8] Intermolecular and intramolecular interactions in conjugated block copolymers drive such self-assembly by the formation of an array of structures ranging from molecular length scales to larger mesostructures in the bulk or at an interface. A number of nanoscale morphologies, such as lamellar, spherical, cylindrical, nanoribbon, or wormlike structures, have been observed in conjugated block copolymers.[6] This inherent tunability will permit the design and fabrication of new components for optoelectronic devices.[9,10]

Regioregular poly(3-hexylthiophene) (rr-P3HT) is a benchmark conjugated polymer for organic field-effect transistors and organic solar cells.[11] Recently, various copolymers containing a polythiophene segment have been designed to selectively align P3HT domains for preferred conduction paths in organic electronics.[12−14] Combining a semiconducting rr-P3HT block with insulating flexible blocks has the potential to generate various highly organized structures resulting from the interplay between *self-assembly* (*e.g.*, $\pi-\pi$ stacking) and *phase separation*, as the balance between thermodynamics and kinetics is altered.[15,16] By changing the physical properties of the nonconjugated segment, it is possible to fine-tune the physical and electrical properties of the copolymer for different device applications.[17−19] For example, when block copolymers are applied in field-effect transistors, these material systems promise the possibility of preferentially segregating the organic semiconductors (P3HT blocks) with long-range order on the gate dielectric, vertically phase separating the insulating blocks on the surface of the active layer leading to self-encapsulation for significant improvements in environmental stability.[20−23] In addition, due to their good bulk charge transport and desirable mechanical properties, rod−coil diblock copolymers that induce highly ordered bulk heterojunction structures by *lateral phase separation* are

* Address correspondence to xiaok@ornl.gov, hongkq@ornl.gov.

Received for review November 8, 2010 and accepted April 1, 2011.

Published online April 01, 2011
10.1021/nn2007964

highly desirable for forming highly efficient and mechanically robust organic solar cells.[24,25] There have been several reports on the synthesis of the "rod−coil" block copolymers that contain a P3HT segment and observations of the microphase separation.[26−29] However, all of the synthesis approaches reported so far involve the polymerization of 3HT first followed by chain extending of the P3HT block with a coil block.[26−29] The resulting block copolymers always have fixed rod (P3HT) length and variable coil length.

The performance of organic field-effect transistors based on those P3HT rod−coil block polymers has also been studied.[30−33] Müller *et al.*[30] reported field-effect transistors based on polyethylene (PE) and rr-P3HT block copolymers with saturated charge carrier mobilities as high as 2×10^{-2} cm^2 V^{-1} s^{-1}. Li and co-workers[31] have demonstrated that rr-P3HT block copolymers are promising materials for use in volatile organic compound (VOC) vapor sensors with greatly enhanced discrimination of different VOCs. However, long-range ordered microstructures in those diblock copolymers composed of polythiophene and a coil-like block have proven difficult to achieve in practice, and the correlation between their self-assembly and their charge carrier transport behavior has not yet been fully demonstrated.

In this contribution, we report the synthesis of polystyrene-*b*-poly(3-hexylthiophene) (PS-*b*-P3HT) block copolymers with fixed PS block length by combined atom transfer radical polymerization (ATRP) and Grignard metathesis (GRIM) polymerization. The resulting nanoscale morphologies of the thin films of these diblock copolymers are studied by various techniques including transmission electron microscopy (TEM), selected area electron diffraction (SAED), grazing-incidence X-ray diffraction (GIXD), and atomic force microscopy (AFM), and additionally by first principles modeling and simulation. These structural characteristics are also correlated with measurements of their charge transport properties configured as field-effect transistors. We find that these block copolymers undergo microphase separation and self-assemble into spherical, lamellar, fibrous, or ribbon nanostructures depending on the P3HT/PS ratios. The surface structures and device characteristics of the conjugated diblock copolymers can be manipulated by processing solvent and thermal annealing temperatures and block copolymer compositions. Unlike the high off-currents of the rr-P3HT diblock copolymer reported in the literature,[32,33] the off-currents of our PS-*b*-P3HT copolymer devices were as small as those measured under strictly inert conditions. Moreover, the highest measured charge mobility, 0.08 cm^2 V^{-1} s^{-1}, for the block copolymer PS-*b*-P3HT containing 85 wt % P3HT is among the highest of all the P3HT-containing, insulating segment diblock copolymers reported in the literature.

RESULTS AND DISCUSSION

4-Bromobenzyl bromide (4-BBB) is a bifunctional initiator: the benzyl bromide moiety is an efficient ATRP initiator under proper conditions, while the bromobenzene part is a good GRIM initiator for the synthesis of conjugated polymers such as 3-hexylthiophene.[34,35] Figure 1a shows the synthesis scheme for the PS-*b*-P3HT diblock copolymers. GPC traces of the PS block and a PS-*b*-P3HT block copolymer (see Figure S1 in Supporting Information) indicate that the synthesis was successful. A series of diblock copolymers with P3HT/PS weight ratios of 85:15, 76:24, 65:35, and 17:83 were synthesized. The compositions of the resulting diblock copolymers are shown in Table 1. For each copolymer, the PS segment was kept constant with a number average molecular weight, M_n, around 2200 g mol^{-1}. The overall composition of the diblock copolymers was controlled by varying the P3HT block lengths. In all cases, the polydispersity index was low (see Table 1), indicating that these block copolymers were well-defined. The single chain structure of a PS-*b*-P3HT diblock copolymer calculated with an AM1 Hamiltonian is shown in Figure 1b.

The optical properties of the polymers were investigated by UV−vis spectroscopy in trichlorobenzene solution and in the solid state (Figure 2). The spectra measured in diluted trichlorobenzene solutions of the PS-*b*-P3HT had one absorption peak at around 450−500 nm and are thereby essentially similar to an rr-P3HT homopolymer. Decreasing the P3HT fraction in the copolymer blue-shifted the position of the main absorption maximum slightly for **P2**−**P4** but significantly for **P1** (with highest PS content). The absorption peaks corresponding to the $\pi-\pi^*$ transitions of the polymers were present at 470 nm in solution and 560 nm in films, respectively (Figure 2b,c). This large red shift (of about 90 nm) suggests the presence of strong intermolecular interactions between the polymer chains (we note that the interaction energy computed from all-electron quantum density functional theory is ∼3 kcal/mol per monomer for P3HT) and the planarization effect of the conjugated polymer backbone, which enables the polymer chains to self-assemble into well-ordered solid-state nanostructures.[36] Semiempirical quantum simulations using the ZINDO/s Hamiltonian with configuration interaction singles (CIS) calculations were used to determine the UV−vis spectrum.[37] These results provide insight into how the polymer chains pack in a thin film and the influence of the PS block. The P3HT−P3HT interchain distance is 0.4 nm (Figure 3). The vertical stacking distance is 1.3 nm (Figure S2 in Supporting Information), in reasonable agreement with the experimental results depicted in Figure 4. The normalized solid-state absorption spectra of all the copolymers, except polymer **P1**, give absorption maxima at 550−570 nm with two shoulders at 520−530 and 600−620 nm. The vibronic splitting of the block copolymers is similar to that seen in rr-P3HT,[33] indicating

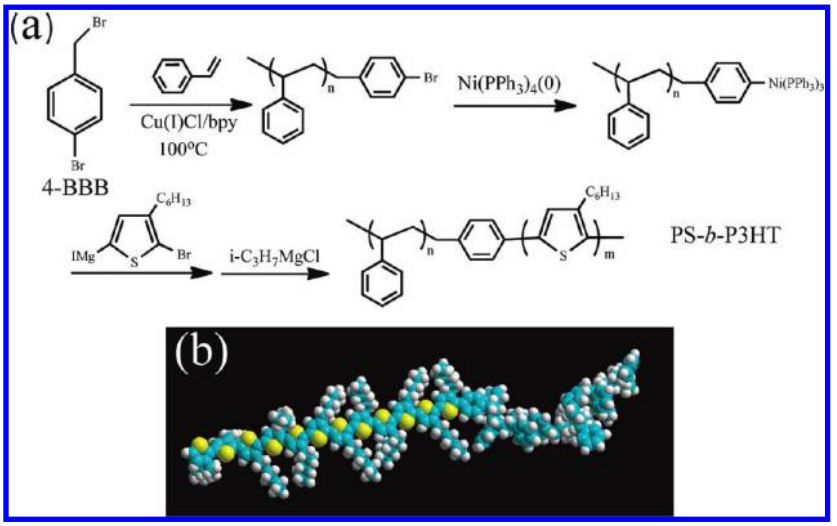

Figure 1. (a) Synthesis scheme for PS-*b*-P3HT diblock copolymer. (b) Semiempirical AM1 Hamiltonian-optimized structure of PS-*b*-P3HT diblock copolymer.

TABLE 1. Polystyrene-*block*-Poly(3-hexylthiophene) Composition

polymer	P3HT (NMR) [mol %]	P3HT (NMR) [wt %]	M_n (NMR)	M_n (GPC) [g mol^{-1}]	PDI (GPC)
P1	11	17	2700	4300	1.21
P2	55	65	6900	9300	1.21
P3	67	76	9600	11300	1.15
P4	76	85	13300	12000	1.32
P3HT[a]	100	100	35500	23000	1.54

[a] Obtained from Merck Chemicals, and the molecular weight data were obtained under our GPC conditions.

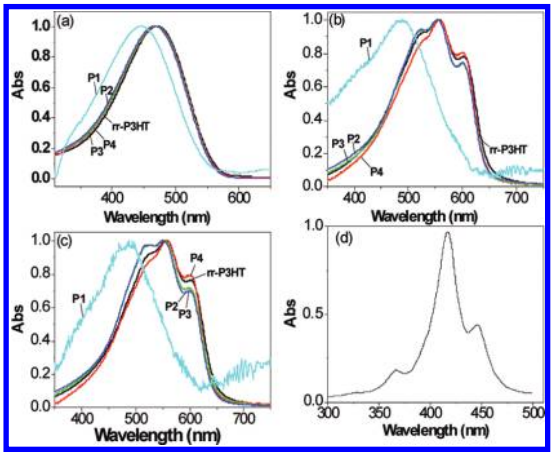

Figure 2. UV–Vis absorption spectra of polymer (normalized intensities) (a) solution in trichlorobenzene, (b) film spin-coated from trichlorobenzene, (c) annealed film at 150 °C spin-coated from trichlorobenzene. (d) Computed UV–vis spectra for a model of 12P3HT–12PS.

the formation of highly ordered structures of lamellar π-stacked aggregates, despite the presence of the PS segment (from simulations, the interchain distance only changes by 0.02 nm going from rr-P3HT to PS-*b*-P3HT). Interestingly, the shoulder in the shorter wavelength region has red-shifted, and the absorbance of the peak in the longer wavelength region increased with increasing P3HT block length. This implies that the polymer with longer P3HT blocks forms an interchain excited state in the ordered films.[38–40] The lack of an absorption shoulder in **P1** is attributed to the large fraction of the insulating amorphous PS block, which induced more random P3HT structures. Surprisingly, the relative intensity of the absorption shoulder in the longer wavelength region for **P4** was even higher than that of the P3HT homopolymer.[38,39] This indicates that the P3HT domains in the **P4** films are better ordered, although the degree of crystallinity of the P3HT fraction is reduced to 85% of the total polymer chain. Therefore, the formation of ordered crystalline P3HT domains was enhanced with the PS segment attached to the P3HT block, resulting in a well-defined microphase-separated nanostructure. After annealing, the absorption spectrum for the film did not change significantly (Figure 2c), indicating the well-organized microstructures of the as-formed thin film.

The computed UV–vis spectrum (Figure 2d) based on the optimized geometry has a peak optical absorption at 436 nm. The shoulder observed in the experimental spectra does not clearly appear and suggests that contributions may also come from long-range interactions between lamellar domains. The shorter wavelength for the absorption maximum compared to experiment could be due to the small chain lengths used in the calculations for the polymers since longer chains have absorption maxima at longer wavelengths (*e.g.*, 24P3HT has an absorption maximum at 532 nm). However, chain packing at constant chain length also red shifts. A smaller number of stacked chains of the same length, 2 chains instead of 3, give the absorption at 502 nm.

The bulk morphology of the block copolymers was characterized by TEM, while the surface morphology of the thin films was characterized using AFM. To ensure the comparability of the surface morphologies and the bulk

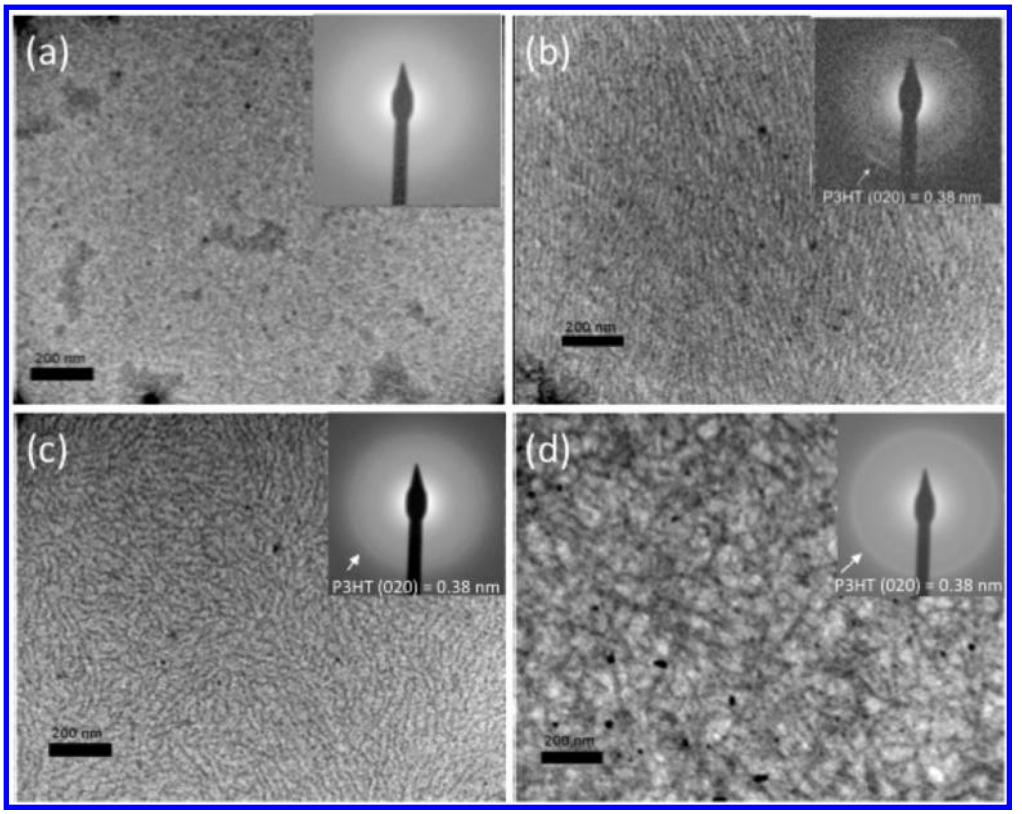

Figure 3. TEM images and SAED patterns (inset) of the self-assembled structures of (a) P1 (spheres), (b) P2 (lamellae), (c) P3 (worm nanofiber), and (d) P4 (crystalline nanoribbon) thin films after annealing.

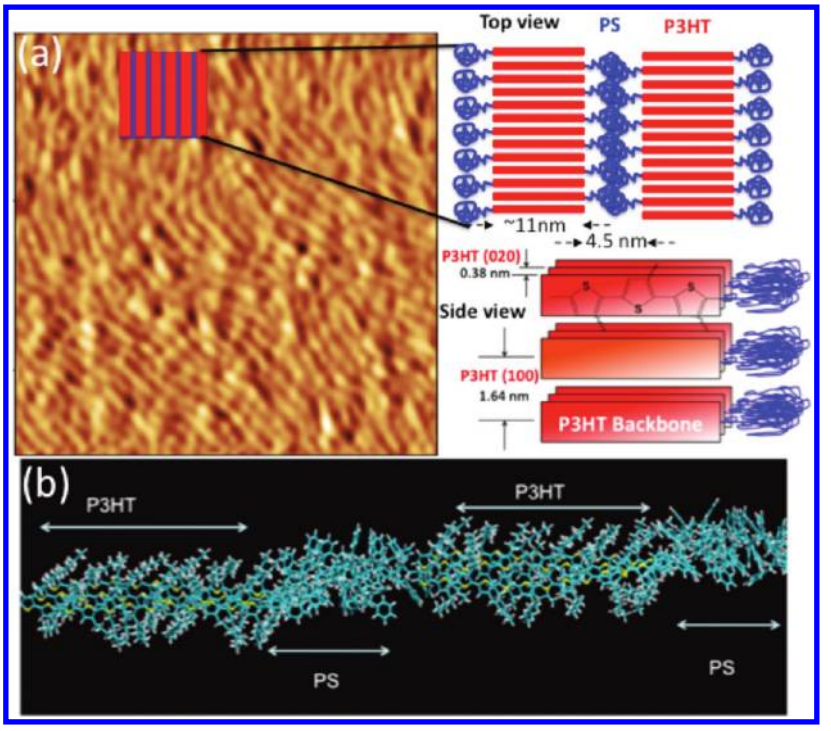

Figure 4. (a) AFM images (500 nm × 500 nm) of the lamellar structure of the P2 film. Inset shows the schematic illustration of the lamellar nanostructures. Left images show the schematic illustrations of the top view and side view of the lamellar structures of the P2 film. (b) Semiempirical AM1 Hamiltonian-optimized lamellar structure of the P2 film.

structures, the same annealing conditions were applied to both types of samples. Before thermal annealing, a flat surface with no phase pattern was observed in as-prepared samples. AFM images were obtained after thermal

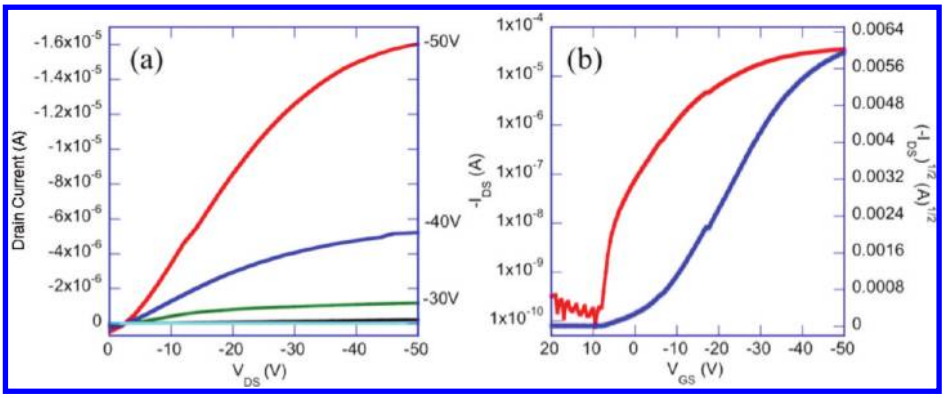

Figure 5. (a) Output characteristics of a bottom contact OFET using P4. (b) Transfer characteristics of the same device at a drain voltage of −40 V.

annealing at several different temperatures for 1 h. As shown in Figure S3 of the Supporting Information, when the annealing temperature was changed from room temperature to 100 °C for **P2**, the sample showed small disordered aggregates with a size of several nanometers. When annealed at 150 °C, AFM images showed clear evidence of lamellar nanostructures. These results indicate that annealing at the temperature above the glass transition temperature of the PS block allows better molecular packing of the P3HT blocks in the forming of thermodynamically stable microphase-separated structures. Figure 3 shows the TEM images of sphere, lamellae, nanofiber, and nanoribbon structures observed for **P1**, **P2**, **P3**, and **P4**, respectively. With increasing P3HT fraction from 17 to 65%, PS-*b*-P3HT self-organized to form spheres (**P1**), lamellae (**P2**), and wormlike nanofibers (**P3**). Furthermore, highly crystalline nanoribbon (**P4**) morphologies are observed, although the strong $\pi-\pi$ interaction between rr-P3HT in the copolymer suppresses the long-range order of the nanostructure. Considering the large difference in crystallinity between PS and P3HT blocks, these nanostructures can be attributed to the interplay between self-assembly (*e.g.*, $\pi-\pi$ stacking of P3HT) and phase separation of the crystalline (P3HT) and amorphous (PS) blocks, a balance between thermodynamics and kinetics. The size of the dark and bright domains in the TEM images depends on the relative ratio of the P3HT and PS blocks. **P2** showed lamellae of the dark domains with a width of about 11 nm, while those with **P3** and **P4** showed longer wormlike and ribbonlike dark domains with widths of around 16 and 25 nm, respectively. On the basis of previous studies of rod−coil block copolymers,[12] the P3HT block forms the fibers (dark regions) while the flexible polystyrene block assembles on either side of the fibers (bright regions). These results clearly suggest that the amorphous PS segment in diblock copolymers plays a significant role in the interfacial crystallinity of P3HT.

GIXD and SAED were used to investigate the structure of these polymer thin films. All of the diblock copolymers displayed typical P3HT (100) and (020) reflections (Figure 3 and Figure S5). GIXD conveniently probes the vertical molecular packing and orientation in the thin film, while transmission mode SAED provides information about in-plane crystallographic packing. The **P2** film showed distinct diffraction peaks at 2θ of 5.3 and 10.6° in the GIXD measurement. These peaks can be assigned to a lamellar layer structure with a lattice constant of 1.69 nm for P3HT. The (020) plane of the P3HT (intermolecular $\pi-\pi$ stacking) was responsible for the outer rings in the SAED patterns of P3HT.[41,42] **P1** shows very weak 100 and 020 patterns because of the large fraction of the amorphous PS block. Remarkably, the SAED pattern of **P2** polymer showed the (020) reflection arcs perpendicular to the lamellar orientation indicative of the long-range order and uniform orientation of the **P2** block copolymer with a lamellar structure. With increasing P3HT content in block copolymers **P3** and **P4**, the intensity and sharpness of the (020) ring are increased, as shown in Figure 3. The high crystallinity of the P3HT block in **P4** was further confirmed by the sharp (020) ring ($\pi-\pi$ stacking) in the SAED pattern, while the nanoribbons from the P3HT block were easily visible in the contrast-enhanced bright-field image. This apparent enhancement in $\pi-\pi$ stacking (despite the presence of the amorphous PS block in the copolymers) is important as such improvement in interfacial order plays significant roles in achieving effective charge transport (Figure 5).[17−19]

From the above morphology and structural analysis, we propose the microphase-separated lamellar structure of **P2** films depicted schematically in Figure 4. As shown in the AFM phase image (Figure 4a), the P3HT and PS blocks self-assemble to form distinct dark and bright domains. The order of those domains improves after annealing. The long-range ordered molecular packing of the crystalline P3HT chains results from the alignment of their alkyl side chains normal to the substrate, with the intermolecular $\pi-\pi$ stacking between the thiophene rings aligned parallel to the substrate in the thin films shown as the red domain in Figure 4. On the other hand, covalently bonded PS blocks phase-separate to form amorphous domains depicted in blue in Figure 4. The other PS-*b*-P3HT polymers containing high contents of P3HT showed similar structural features after thermal annealing of the films but formed fiberlike morphology

(Figure S5 in Supporting Information). Similar to other previously reported P3HT polymers, these ordered structures are favorable for enhanced charge transport in a FET device geometry.[17−19]

To measure the field-effect mobility, we recorded transfer curves in the saturation regime at $V_{DS} = -50$ V and calculated the mobility from the slope of a line drawn through the linear part of an $I_{DS}^{1/2}$ *versus* V_G plot as shown in Figure 5. Table 2 reports the field-effect mobilities for all of the studied polymers. In all cases, we report the highest mobility measured, along with the average mobility of at least 10 transistors. In view of the high content of the insulating PS block and the absence of a well-ordered P3HT phase in thin film **P1**, not unexpectedly, very small source−drain currents at the detection limit were recorded in field-effect transistor configurations for this diblock copolymer. Carrier mobilities in the **P1** films were estimated to be less than 10^{-5} cm^2/(V·s). This poor mobility in a device of **P1** is very different than a previous report for a P3HT/PS blended system,[43,44] where even extremely small (1 wt %) fractions of P3HT can have mobilities as high as that of the pure P3HT homopolymer. This is because the two phases (P3HT *vs* PS) separate in a slightly different fashion in the blend from that in block copolymer systems. The copolymers do not permit large-scale phase separation, thus providing percolating charge transport pathways in the bulk. In blends, the two components will separate on a much larger scale, possibly resulting in enrichment of the semiconductor at the interface. As a consequence, a FET performance identical to that of neat rr-P3HT homopolymer devices may be found in blends with very high PS concentrations; however, it is difficult to achieve for a PS-*b*-P3HT diblock copolymer with high PS content. On the other hand, FETs with excellent electronic performances were obtained with **P2** diblock copolymer films. Clear p-type transistor action with current modulations of 10^4-10^5 and charge carrier mobilities of up to 0.03 cm^2/(V·s) were measured for devices based on **P2** thin film because of the ordered lamellar structures. Charge transfer integrals which are related to carrier mobility (as given by the Marcus formula for the electron transfer rate) were determined using Koopman's theorem (while this is an approximation, the values are often quite reasonable[45] for the system, but with only 3 chains), giving 0.11 eV for hole transport. This is a modest transfer integral, but it does suggest a reasonable electronic coupling for this system, in agreement with the higher charge carrier mobility. The **P3** polymer has a little lower measured mobility (around 0.02 cm^2/(V·s)) because of the random, short-range ordered nanofiber structures as shown in Table 2. Remarkably, **P4** (85 wt % P3HT) with the highly crystalline nanoribbon structures in the film, displayed significantly enhanced charge transport properties as compared to the P3HT homopolymer, with up to a factor of 2 increase in measured mobility (0.08 cm^2/(V·s)). This is a rather surprising observation. The origin of this enhanced charge transport perhaps results from an improved ordered P3HT domain in the presence of a low content of the flexible PS segment (15%) in the block copolymer. This is confirmed by the fact that the relative intensities of the absorption shoulder in the UV−vis spectra for **P4** was even higher than that for the P3HT homopolymer. Figure S6 in Supporting Information shows the dependence of the field-effect mobility on annealing temperature for diblock copolymer devices. The mobility is improved by increasing the annealing temperature to 150 °C because the traps and/or stress defects in the ordered and crystalline phase of P3HT in the diblock copolymer films are removed after annealing.

In a series of devices based on various PS-*b*-P3HT block copolymers as well as P3HT homopolymer (all devices prepared and measured under the same

TABLE 2. Summary of All Field Effects Measured for rr-P3HT and for the Block Copolymer Series

		mobility			
polymer	P3HT [wt%]	μ^{max} [cm^2/(V·s)]	μ^{avg} [cm^2/(V·s)]	on/off ratio	threshold voltage [V]
P1	17	0.00005	0.00004	1×10^3	20 to 25
P2	65	0.032	0.028	2×10^6	−2 to −8
P3	76	0.018	0.012	3×10^5	−2 to 6
P4	85	0.083	0.065	1×10^5	−5 to 10
rr-P3HT	100	0.046	0.041	8×10^3	16 to 25

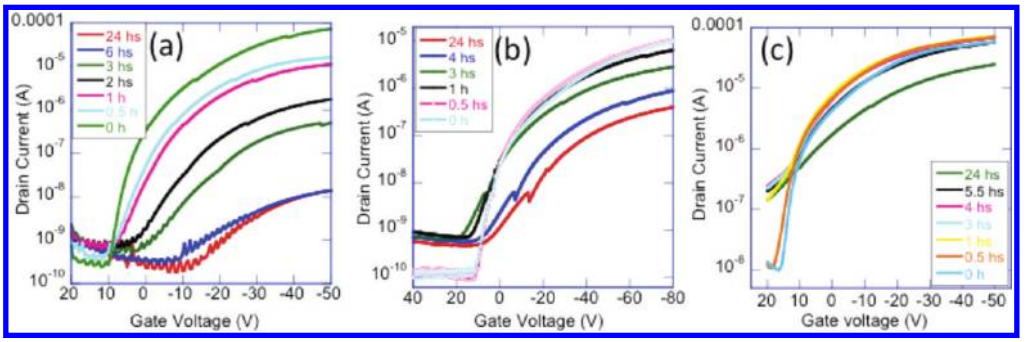

Figure 6. Environmental stability of (a) P2, (b) P4-based, and (c) P3HT-based OFET. Devices based on diblock copolymers with a low concentration of P3HT show significantly improved environmental stability when compared with those comprising neat P3HT, which are known to show doping-induced instabilities on exposure to air and light.

conditions), we found that the threshold voltage decreased from more than 18 V for P3HT homopolymer to about 4 V for **P2** (65 wt % P3HT) (Table 2). Concomitantly, the on/off ratio increased significantly from 10^3 for P3HT homopolymer to up to 10^6 for **P2** (65 wt % P3HT), resulting from the introduction of the insulating PS block into the conductive network. The device performances including mobility, threshold voltage, and on/off ratio of the PS-*b*-P3HT diblock copolymer films from various processing solvents were significantly improved using solvents that had higher boiling points, as shown in Figure S7 in Supporting Information.

Finally, we find that the device performances of FETs based on the copolymers showed significant improvement in environmental stability after exposure of the devices to light and air when compared with those comprising P3HT homopolymer (see Figure 6). Despite the lack of a vertical phase separation mechanism for these diblock copolymers, which is known to result in "self-encapsulation" benefits, clearly, the added insulator block may be the origin of this beneficial attribute. Further investigations are required to elucidate this in more detail.

CONCLUSIONS

In summary, we have investigated the correlations between the self-assembled structures of different P3HT-*b*-PS block copolymers and their field-effect charge transport behaviors. We found that these block copolymers were able to undergo microphase separation and self-assemble into nanostructures displaying sphere, lamellae, nanofiber, or nanoribbon morphologies depending on the amount of P3HT fractions. The introduction of a flexible PS block enhanced the chain packing of P3HT domains and thus tuned the self-assembled morphologies of the block copolymers. Moreover, a nonconjugated PS block provides good solubility and mechanical properties. The morphologies and interfacial crystallinity of P3HT in diblock copolymers play significant roles in the performance of organic thin film transistor devices. The spin-cast PS-*b*-P3HT diblock copolymer films all developed $\pi-\pi$ stacking parallel to the substrate surface, which is optimal for transport in field-effect transistors. Remarkably, **P4** (85 wt % P3HT) displayed significantly enhanced charge transport properties as compared to the P3HT homopolymer, with up to a factor of 2 increase in measured mobility (0.08 $cm^2/(V \cdot s)$). This enhancement can be attributed to the highly crystalline, ordered P3HT domains in the thin films. The PS-b-P3HT device performances including mobility, threshold voltage, on/off ratio, and environmental stability were significantly improved compared to that of the rr-P3HT homopolymer. Through the variation of the length of the rod segment (P3HT) in these block copolymers morphology control and fine-tuning of their charge properties were achieved. We believe that these results open additional avenues for the improvement of organic electronic devices.

EXPERIMENTAL SECTION

Materials. All chemicals were purchased from Sigma-Aldrich and used as received without further purification unless otherwise stated. Anisole, tetrahydrofuran (THF), and dichloromethane were freshly distilled from calcium hydride before use. 4-Bromobenzyl bromide (4-BBB) was recrystallized from saturated methanol solution. Hexanes and toluene were stirred over sodium and distilled under inert conditions before use. Styrene was washed with an aqueous sodium hydroxide solution and distilled over calcium hydride under reduced pressure. Lithium chloride and $Ni(PPh_3)_4(0)$ were dissolved in THF and sealed into ampules with final concentrations of 0.24 and 9.0×10^{-5} mol/L, respectively. 2-Bromo-3-hexyl-5-iodine thiophene and its Grignard reagent were synthesized according to the procedure described by Yokoyama *et al.*[29]

Synthesis of PS Block by Atom Transfer Radical Polymerization. 4-Bromobenzene-functionalized polystyrene was synthesized by ATRP using 4-BBB, Cu(I)Cl, and the 2,2′-bipyridyl initiating system in anisole. The molar ratio of the polymerization mixture was [St]/[CuCl]/[bpy]/[4-BBB] = 100:1:2:1. After three freeze−pump−thaw cycles, the mixture was sealed under vacuum and kept in an oil bath with temperature at 100 °C. The polymerization was quenched after 12 h by cooling the reaction tube rapidly in ice water. The heterogeneous solution was then passed through a neutral alumina column and precipitated into excess methanol. The functionalized PS was recovered by filtration and dried under vacuum for 24 h.

Synthesis of PS-*b*-P3HT Block Copolymers. The polymerizations were carried out under high vacuum in custom-made glass reactors equipped with break-seals and constrictions, which are used for the addition of reagents or removal of intermediate products, respectively. A typical procedure for synthesis of PS-*b*-P3HT is as follows: 1.00 g of 4-BBB-functionalized polystyrene was added to the reactor and dried under high vacuum for 2 h. Then ~3.8 mL of LiCl/THF solution and 3 mL of $Ni(PPh_3)_4(0)$ THF solution were added to the reactor *via* break-seal techniques. After removing the solvent (THF) under vacuum, 15 mL of toluene was distilled into the reactor through inline distillation followed by stirring for 48 h at room temperature to ensure the insertion of Ni complexes into the C−Br bond. Then 120 mL of hexanes was distilled into the reaction mixture to precipitate the polymer. After inline filtration, solvent mixture containing excess unreacted nickel catalyst was collected into one of the glass ampules connected to the reactor through constriction and removed from the reactor. The precipitated polymer complex was washed with hexanes three more times to remove the excess nickel catalyst completely and then dissolved in ~20 mL of THF. Predetermined amounts of LiCl/THF and 2-bromo-3-hexyl-5-magnesium iodide thiophene were introduced from ampules, and the polymerization was allowed to proceed at room temperature overnight. The polymerization was quenched by adding isopropylmagnesium chloride solution. The polymer was purified by Soxhlet extractions using methanol, hexanes, toluene, tetrahydrofuran, and chloroform and then dried at 40 °C under vacuum to constant weight.[15] rr-P3HT homopolymers were synthesized using GRIM method and purified through subsequent solvent extractions.

Characterization. Molecular weights and polydispersity index (PDI) of the polymers were obtained using a Waters Alliance GPC system equipped with a Waters 2695 pump, a Waters 2414 refractive index detector, Wyatt MiniDAWN light scattering detector, and three Polymer Laboratories Mixed-B styragel columns. THF was used as the eluent (1 mL/min), and the temperature was controlled at 35 °C. Linear polystyrene standards were used for calibration. ^1H NMR spectra were obtained on Varian VNMR 500

spectrometer using tetramethylsilane (0.00 ppm) as internal standard. UV–Vis spectra were recorded on a Cary 5000 spectrometer from the diluted trichlorobenzene solution and polymer thin films on quartz substrates. The surface morphologies of the spun-cast polymer films were observed on Asylum MFP AFM. GIXD analysis was performed with spin-coated films on Si wafer substrates by using a PANalytical X'pert Pro powder diffractometer with Cu Kα radiation. TEM images were obtained from a Tecnai 20 transmission electron microscope, and the samples were prepared by directly drop-casting PS-*b*-P3HT solution on carbon-coated grids to observe its stand-alone morphology and crystal structure. SAED patterns were calibrated against Au(111) standards (0.2335 nm).

Charge Mobility Measurement. Organic field-effect transistors were fabricated in the bottom contact configurations on heavily doped n-type Si substrates which served as the gate and 100 nm of thermally grown silicon dioxide as the dielectric layer. The source and drain electrodes were patterned using standard photolithography methods followed by sequential e-beam deposition of *ca.* 10 nm of Ti and 60 nm of Au. The channel lengths were 5 to 50 μm, and the channel widths were 500 and 1000 μm. The polymer films were spun-coated in air from 10 mg/mL trichlorobenzene solution and annealed in a vacuum oven at different temperatures for 1 h. The polymer solutions were filtered through 0.2 μm PTFE filters prior to film deposition. Electrical measurements were made in air using a Keithley 4200 semiconductor parameter analyzer and a probe station.

Acknowledgment. This research was conducted at the Center for Nanophase Materials Sciences, which is sponsored at Oak Ridge National Laboratory by the Scientific User Facilities Division, U.S. Department of Energy.

Supporting Information Available: Figures showing the GPC traces for PS block and a PS-*b*-P3HT block copolymer and its ^{1}H NMR spectrum, a modeled structure of a vertically packed domains of PS-*b*-P3HT lamellae, AFM phase images and XRD patterns of **P2** spin-coated films on SiO_2 substrates after annealing at various temperatures, XRD patterns of all PS-*b*-P3HT diblock copolymers drop-casting films on Si substrates, AFM phase images and XRD patterns of **P4** spin-coated films on SiO_2 substrates after annealing at various temperatures, field-effect mobility of **P2**, **P3**, and **P4** block copolymers after annealing at different annealing temperatures, and field-effect mobility of **P4** thin films prepared from different solvents along with the description of the methodology for modeling and simulation. This material is available free of charge *via* the Internet at http://pubs.acs.org.

REFERENCES AND NOTES

1. Sirringhaus, H.; Brown, P. J.; Friend, R. H.; Nielsen, M. M.; Bechgaard, K.; Langeveld-Voss, B. M. W.; Spiering, A. J. H.; Janssen, R. A. J.; Meijer, E. W.; Herwig, P.; *et al*. Two-Dimensional Charge Transport in Self-Organized, High-Mobility Conjugated Polymers. *Nature* **1999,** *401*, 685–688.
2. Bao, Z.; Lovinger, A. J.; Dodabalapur, A. Organic Field-Effect Transistors with High Mobility Based on Copper Phthalocyanine. *Appl. Phys. Lett.* **1996,** *69*, 3066–3068.
3. Sun, Y.; Liu, Y.; Zhu, D. Advances in Organic Field-Effect Transistors. *J. Mater. Chem.* **2005,** *15*, 53–65.
4. Li, G.; Shrotriya, V.; Huang, J.; Yao, Y.; Moriarty, T.; Emery, K.; Yang, Y. High-Efficiency Solution Processable Polymer Photovoltaic Cells by Self-Organization of Polymer Blends. *Nat. Mater.* **2005,** *4*, 864–868.
5. Ma, W.; Yang, C.; Gong, X.; Lee, K.; Heeger, A. J. Thermally Stable, Efficient Polymer Solar Cells with Nanoscale Control of the Interpenetrating Network Morphology. *Adv. Funct. Mater.* **2005,** *15*, 1617–1622.
6. Segalman, R. A.; McCulloch, B.; Kirmayer, S.; Urban, J. J. Block Copolymers for Organic Optoelectronics. *Macromolecules* **2009,** *42*, 9205–9216.
7. Sommer, M.; Lindner, S. M.; Thelakkat, M. Microphase-Separated Donor–Acceptor Diblock Copolymers: Influence of HOMO Energy Levels and Morphology on Polymer Solar Cells. *Adv. Funct. Mater.* **2007,** *17*, 1493–1500.
8. Sommer, M.; Huttner, S.; Wunder, S.; Thelakkat, M. Electron-Conducting Block Copolymers: Morphological, Optical, and Electronic Properties. *Adv. Mater.* **2008,** *20*, 2523–2527.
9. Scherf, U.; Gutacker, A.; Koenen, N. All-Conjugated Block Copolymers. *Acc. Chem. Res.* **2008,** *41*, 1086–1097.
10. Liang, Y.; Wang, H.; Yuan, S.; Lee, Y.; Gan, L.; Yu, L. Conjugated Block Copolymers and Co-Oligomers: From Supramolecular Assembly to Molecular Electronics. *J. Mater. Chem.* **2007,** *17*, 2183–2194.
11. Zhang, R.; Li, B.; Iovu, M. C.; Jeffries-El, M.; Sauve, G.; Cooper, J.; Jia, S.; Tristram-Nagle, S.; Smilgies, D. M.; Lambeth, D. N.; *et al*. Nanostructure Dependence of Field-Effect Mobility in Regioregular Poly(3-hexylthiophene) Thin Film Field Effect Transistors. *J. Am. Chem. Soc.* **2006,** *128*, 3480–3481.
12. Wu, P.; Ren, G.; Kim, F. S.; Li, C.; Mezzenga, R.; Jenekhe, S. A. Poly(3-hexylthiophene)-*b*-Poly(3-cyclohexylthiophene): Synthesis, Microphase Separation, Thin Film Transistors, and Photovoltaic Applications. *J. Polym. Sci., Part A: Polym. Chem.* **2010,** *48*, 614–626.
13. Chueh, C.; Higashihara, T.; Tsai, J.; Ueda, M.; Chen, W. All-Conjugated Diblock Copolymer of Poly(3-hexylthiophene)-*block*-Poly(3-phenoxymethylthiophene) for Field-Effect Transistor and Photovoltaic Applications. *Org. Electron.* **2009,** *10*, 1541–1548.
14. Zhang, Y.; Tajima, K.; Hirota, K.; Hashimoto, K. Synthesis of All-Conjugated Diblock Copolymers by Quasi-Living Polymerization and Observation of Their Microphase Separation. *J. Am. Chem. Soc.* **2008,** *130*, 7812–7813.
15. Alemseghed, M. G.; Gowrisanker, S.; Servello, J.; Stefan, M. C. Synthesis of Di-block Copolymers Containing Regioregular Poly(3-hexylthiophene) and Poly(tetrahydrofuran) by a Combination of Grignard Metathesis and Cationic Polymerizations. *Macromol. Chem. Phys.* **2009,** *210*, 2007–2014.
16. Iovu, M. C.; Zhang, R.; Cooper, J. R.; Smilgies, D. M.; Javier, A. E.; Sheina, E. E.; Kowalewski, T.; McCullough, R. D. Conducting Block Copolymers of Regioregular Poly(3-hexylthiophene) and Poly(methacrylates): Electronic Materials with Variable Conductivities and Degrees of Interfibrillar Order. *Macromol. Rapid Commun.* **2007,** *28*, 1816–1824.
17. Surin, M.; Coulembier, O.; Tran, K.; Winter, J.; Leclere, P.; Gerbaux, P.; Lazzaroni, R.; Dubois, P. Regioregular Poly(3-hexylthiophene)–Poly(ε-caprolactone) Block Copolymers: Controlled Synthesis, Microscopic Morphology, and Charge Transport Properties. *Org. Electron.* **2010,** *11*, 767–774.
18. Botiz, I.; Darling, S. B. Self-Assembly of Poly(3-hexylthiophene)-*block*-Polylactide Block Copolymer and Subsequent Incorporation of Electron Acceptor Material. *Macromolecules* **2009,** *42*, 8211–8217.
19. Radano, C. P.; Scherman, O. A.; Stingelin-Stutzmann, N.; Muller, C.; Breiby, D. W.; Smith, P.; Janssen, R. A. J.; Meijer, E. W. Crystalline-Crystalline Block Copolymers of Regioregular Poly(3-hexylthiophene) and Polyethylene by Ring-Opening Metathesis Polymerization. *J. Am. Chem. Soc.* **2005,** *127*, 12502–12503.
20. Olsen, B. D.; Li, X.; Wang, J.; Segalman, R. A. Thin Film Structure of Symmetric Rod–Coil Block Copolymers. *Macromolecules* **2007,** *40*, 3287–3295.
21. Olsen, B. D.; Alcazar, D.; Krikorian, V.; Toney, M. F.; Thomas, E. L.; Segalman, R. A. Crystalline Structure in Thin Films of DEH-PPV Homopolymer and PPV-*b*-PI Rod–Coil Block Copolymers. *Macromolecules* **2008,** *41*, 58–66.
22. Arias, A. C.; Endicott, F.; Street, R. A. Surface-Induced Self-Encapsulation of Polymer Thin-Film Transistors. *Adv. Mater.* **2006,** *18*, 2900–2904.
23. Goffri, S.; Muller, C.; Stingelin-Stutzmann, N.; Breiby, D. W.; Radano, C. P.; Andreasen, J. W.; Thompson, R.; Janssen, R. A. J.; Nielsen, M. M.; Smith, P.; *et al*. Multicomponent Semiconducting Polymer Systems with Low Crystallization-Induced Percolation Threshold. *Nat. Mater.* **2006,** *5*, 950–956.
24. Zhang, Q.; Cirpan, A.; Russell, T. P.; Emrick, T. Donor–Acceptor Poly(thiophene-*block*-perylene diimide) Copolymers: Synthesis and Solar Cell Fabrication. *Macromolecules* **2009,** *42*, 1079–1082.

25. Ren, G.; Wu, P.; Jenekhe, S. A. Enhanced Performance of Bulk Heterojunction Solar Cells Using Block Copoly(3-alkylthiophene)s. *Chem. Mater.* **2010,** *22*, 2020–2026.
26. Liu, J.; Sheina, E.; Kowalewski, T.; McCullough, R. D. Tuning the Electrical Conductivity and Self-Assembly of Regioregular Polythiophene by Block Copolymerization: Nanowire Morphologies in New Di- and Triblock Copolymers. *Angew. Chem., Int. Ed.* **2002,** *41*, 329–332.
27. Iovu, M. C.; Jeffries-El, M.; Zhang, R.; Kowalewski, T.; McCullough, R. D. Conducting Block Copolymer Nanowires Containing Regioregular Poly(3-hexylthiophene) and Polystyrene. *J. Macromol. Sci., Pure Appl. Chem.* **2006,** *43*, 1991–2000.
28. Dai, C.; Yen, W.; Lee, Y.; Ho, C.; Su, W. Facile Synthesis of Well-Defined Block Copolymers Containing Regioregular Poly(3-hexyl thiophene) *via* Anionic Macroinitiation Method and Their Self-Assembly Behavior. *J. Am. Chem. Soc.* **2007,** *129*, 11036–11038.
29. Yokoyama, A.; Miyakoshi, R.; Yokozawa, T. Chain-Growth Polymerization for Poly(3-hexylthiophene) with a Defined Molecular Weight and a Low Polydispersity. *Macromolecules* **2004,** *37*, 1169–1171.
30. Müller, C.; Goffri, D.; Breiby, D. W.; Andreasen, J. W.; Chanzy, H. D.; Janssen, R. A. J.; Nielsen, M. N.; Radano, C. P.; Sirringhaus, H.; Smith, P.; *et al*. Tough, Semiconducting Polyethylene−Poly(3-hexylthiophene) Diblock Copolymers. *Adv. Funct. Mater.* **2007,** *17*, 2674–2679.
31. Li, B.; Sauve, G.; Iovu, M. C.; Jeffries-EL, M.; Zhang, R.; Cooper, J.; Santhanam, S.; Schultz, L.; Revelli, J. C.; Kusne, A. G.; *et al*. Volatile Organic Compound Detection Using Nanostructured Copolymers. *Nano Lett.* **2006,** *6*, 1598–1602.
32. Sauve, G.; McCullough, R. D. High Field-Effect Mobilities for Diblock Copolymers of Poly(3-hexylthiophene) and Poly(methyl acrylate). *Adv. Mater.* **2007,** *19*, 1822–1825.
33. Sauve, G.; Zhang, R.; Jia, S.; Kowalewski, T.; McCullough, R. D. Synthesis, Mobility, and Conductivity of Well-Defined Regioregular Poly(3-hexylthiophene) and Diblock Copolymers of Regioregular Poly(3-hexylthiophene). *Proc. SPIE* **2006,** *6336*, U164–U172.
34. Coessens, V.; Pintauer, T.; Matyjaszewski, K. Functional Polymers by Atom Transfer Radical Polymerization. *Prog. Polym. Sci.* **2001,** *26*, 337–377.
35. Iovu, M. C.; Sheina, E. E.; Gil, R. R.; McCullough, R. D. Experimental Evidence for the Quasi-"Living" Nature of the Grignard Metathesis Method for the Synthesis of Regioregular Poly(3-alkylthiophenes). *Macromolecule* **2005,** *38*, 8649–8656.
36. Kim, D. H.; Lee, B.; Moon, H.; Kang, H. M.; Jeong, E. J.; Park, J.; Han, K.; Lee, S.; Yoo, B. W.; Koo, B. W.; *et al*. Liquid-Crystalline Semiconducting Copolymers with Intramolecular Donor−Acceptor Building Blocks for High-Stability Polymer Transistors. *J. Am. Chem. Soc.* **2009,** *131*, 6124–6132.
37. Sumpter, B. G.; Kumar, P.; Mehta, A.; Barnes, M. D.; Shelton, W. A.; Harrison, R. J. Computational Study of the Structure, Dynamics, and Photophysical Properties of Conjugated Polymers and Oligomers Under Nanoscale Confinement. *J. Phys. Chem. B* **2005,** *109*, 7671–7685.
38. Zhang, Y.; Tajima, K.; Hashimoto, K. Nanostructure Formation in Poly(3-hexylthiophene-*block*-3-(2-ethylhexyl)thiophene)s. *Macromolecules* **2009,** *42*, 7008–7015.
39. Brown, P. J.; Thomas, D. S.; Kohler, A.; Wilson, J. S.; Kim, J. S.; Ramsdale, C. M.; Sirringhaus, H.; Friend, R. H. Effect of Interchain Interactions on the Absorption and Emission of Poly(3-hexylthiophene). *Phys. Rev. B* **2003,** *67*, 064203.
40. Kline, R. J.; McGehee, M. D.; Kadnikova, E. N.; Liu, J. S.; Frechet, J. M. J; Toney, M. F. Dependence of Regioregular Poly(3-hexylthiophene) Film Morphology and Field-Effect Mobility on Molecular Weight. *Macromolecules* **2005,** *38*, 3312–3319.
41. Kline, R. J.; McGehee, M. D.; Toney, M. F. Highly Oriented Crystals at the Buried Interface in Polythiophene Thin-Film Transistors. *Nat. Mater.* **2006,** *5*, 222–228.
42. Yang, X.; van Duren, J. K. J.; Janssen, R. A. J.; Michels, M. A. J.; Loos, J. Morphology and Thermal Stability of the Active Layer in Poly(*p*-phenylenevinylene)/Methanofullerene Plastic Photovoltaic Devices. *Macromolecules* **2004,** *37*, 2151–2158.
43. Qiu, L.; Lee, W. H.; Wang, X.; Kim, J. S.; Lim, J. A.; Kwak, D.; Lee, S.; Cho, K. Organic Thin-Film Transistors Based on Polythiophene Nanowires Embedded in Insulating Polymer. *Adv. Mater.* **2009,** *21*, 1349–1353.
44. Kumar, A.; Baklar, M. A.; Scott, K.; Kreouzis, T.; Stingelin-Stutzmann, N. Efficient, Stable Bulk Charge Transport in Crystalline/Crystalline Semiconductor-Insulator Blends. *Adv. Mater.* **2009,** *21*, 4447–4451.
45. Vazquez-Mayagoitia, A.; Huertas, O.; Brancolini, G.; Migliore, A.; Sumpter, B. G.; Orozco, M.; Luque, F. J.; Di Felice, R.; Fuentes-Cabrera, M. *Ab Initio* Study of the Structural, Tautomeric, Pairing, and Electronic Properties of Seleno-Derivatives of Thymine. *J. Phys. Chem. B* **2009,** *113*, 14465–14472.